Chiral Phonons at High-Symmetry Points in Monolayer Hexagonal Lattices

Lifa Zhang and Qian Niu

Phys. Rev. Lett. **115**, 115502 — Published 11 September 2015

DOI: 10.1103/PhysRevLett.115.115502

Chiral phonons at high-symmetry points in monolayer hexagonal lattices

Lifa Zhang[1,2] and Qian Niu[1,3]

[1]*Department of Physics, The University of Texas at Austin, Austin, Texas 78712, USA*
[2]*Department of Physics and Institute of Theoretical Physics, Nanjing Normal University, Nanjing, 210023, China*
[3]*International Center for Quantum Materials, Peking University, Beijing 100871, China*

In monolayer hexagonal lattices, the intravalley and intervalley scattering of electrons can involve chiral phonons at Brillouin-zone center and corners, respectively. At these high-symmetry points, there is a three-fold rotational symmetry endowing phonon eigenmodes with a quantized pseudo angular momentum, which includes orbital and spin parts. Conservation of pseudo angular momentum yields selection rules for intravalley and intervalley scattering of electrons by phonons. Concrete predictions of helicity resolved optical phenomena are made on monolayer molybdenum disulfide. The chiral phonons at Brillouin-zone corners excited by polarized photons can be detected by a valley phonon Hall effect. The chiral phonons, together with phonon circular polarization, phonon pseudo angular momentum, selection rules, and valley phonon Hall effect will extend the basis for valley-based electronics and phononics applications in the future.

PACS numbers: 63.22.-m, 72.10.Di, 72.90.+y

Due to inversion symmetry breaking, valley-contrasting electronic physics proposed by Xiao *et al.* in 2007 [1] has attracted a growing interest in the manipulation of the valley degree of electrons since it has potential applications in valley-dependent optoelectronics [2] and coupled spin and valley physics [3]. Besides charge and spin, separated valleys in momentum space constitute another discrete degrees of freedom for electrons with long relaxation time, which leads to emergence of valleytronics, such as valley polarization, valley current, and valley coherence on transition-metal dichalcogenides (TMD) materials [4–10]. The valley electron interband scattering involves a polarized photoexcitation and photoluminescence; however, the intervalley electron scattering will involve Brillouin-zone-corner (valley) phonons [7]. Given the fact that electrons have definite chirality at valleys, a natural question then arises: whether do valley phonons have chirality and how does the chirality play a role in electronic intervalley scattering?

Very recently, the helicity-resolved Raman scattering has experimentally observed in TMD atomic layers[11], where the authors found Brillouin-zone-center ($\mathbf{\Gamma}$) phonons can completely reverse the helicity of incident photons. Such finding implies that besides the valley phonons, the $\mathbf{\Gamma}$ phonons involved in the intravalley scattering of electrons can also have chirality. Therefore, it is highly desirable to investigate phonon chirality at these high-symmetry points in Brillouin zone of the hexagonal lattices and their applications in valleytronics.

In this Letter, we observe chiral phonons at Brillouin-zone center and corners of honeycomb lattices. The three-fold rotational symmetry at these high-symmetry points allows us to label phonon eigenmodes with pseudo angular momentum (PAM). The lack of inversion symmetry within the plane and the fact that time reversal symmetry is broken at $\boldsymbol{K}$ and $\boldsymbol{K}'$ points are the fundamental reasons why valley phonon modes are non-degenerate and have definite PAM. At the $\mathbf{\Gamma}$ point where time reversal symmetry is presented, phonon modes with opposite pseudo angular momenta become degenerate. The chirality of phonons at these high-symmetry points not only decides the selection rules in both intravalley and intervalley electronic scattering but also can endow phononics with other potential effects, e.g., valley phonon Berry curvature and valley phonon Hall effect. And near these high-symmetry points phonon has extremes in dispersion and thus a large density of states. Therefore chiral phonons will play an important role in valleytronics, especially in intravalley or intervalley scattering of electrons or holes.

Chirality of phonons. To study chiral phonons, we first focus on a two-dimensional honeycomb lattice model, where each unit cell has two sublattices A and B. The honeycomb AB lattice can serve as a simplified model to demonstrate general features of chiral phonons in monolayer materials, such as gapped graphene with isotopic doping [12] or staggered sublattice potential [13], hexagonal boron nitride[14]. From calculated eigenvectors, we can plot sublattice vibrations at valleys as shown in the insets of Fig. 1(a). At valleys, all the vibrations are circularly polarized. For valley phonon modes of band 1 and 4, the two sublattices do opposite circular motions; for band 2 and 3 while one sublattice is still the other sublattice does a circular motion. From valley $\boldsymbol{K}$ to $\boldsymbol{K}'$, all the circular motions will change to opposite directions, thus in latter discussion we will focus on one of the valleys while results at the other one are achieved by time reversal symmetry.

The phonon chirality can be characterized by polarization of phonons, which comes from the circular vi-

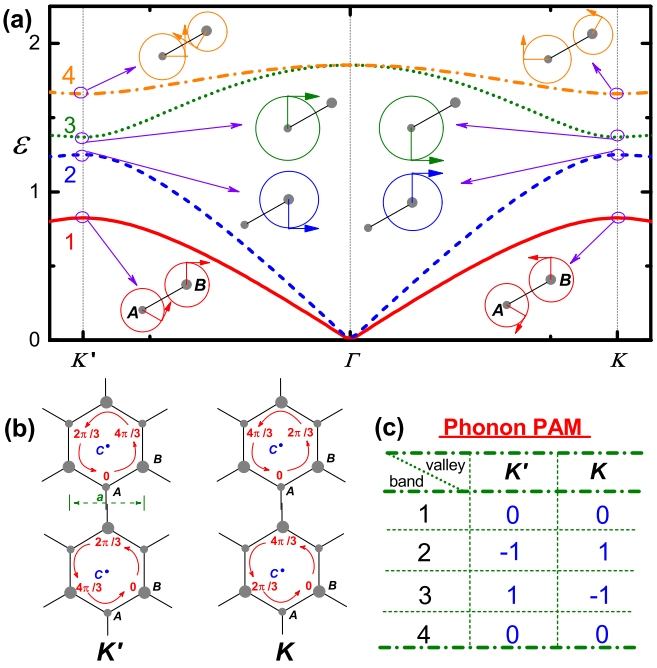

band \ valley	K'	K
1	0	0
2	-1	1
3	1	-1
4	0	0

FIG. 1: **Valley phonons in a honeycomb AB lattice.** (a) Phonon dispersion relation of a honeycomb AB lattice. The insets show phonon vibrations for sublattices A and B in one unit cell at $\boldsymbol{K'}$ ($k_x = -\frac{4\pi}{3a}, k_y = 0$) and $\boldsymbol{K}$ ($k_x = \frac{4\pi}{3a}, k_y = 0$), numbers 1 to 4 denote four bands. The radii of circles denote vibration amplitudes; phase and rotation direction are included. (b) Phase correlation of phonon non-local part for sublattice A (upper two panels) and sublattice B (lower two panels) at (K') (left) and $\boldsymbol{K}$ (right). (c) Phonon pseudo angular momentum (PAM) for bands 1 to 4 at valleys $\boldsymbol{K'}$ and $\boldsymbol{K}$. Here, the longitudinal spring constant $K_L = 1$, the transverse one $K_T = 0.25$, and $m_A = 1$, $m_B = 1.2$. The primitive vectors are $(a, 0)$ and $(a/2, \sqrt{3}a/2)$, and the phonon energy ε equals to $\hbar\omega_{\rm ph}$

.

bration of sublattices. To consider the polarization along z direction, we look at the phonon eigenvectors $\epsilon = (x_1\ y_1\ x_2\ y_2)^T$ (here we take a two-sublattice unit cell as an example, for a general case see Supplementary information Sec. I [15]). By defining a new basis where one sublattice has right-handed or left-handed circular polarization as $|R_1\rangle \equiv \frac{1}{\sqrt{2}}(1\ i\ 0\ 0)^T$; $|L_1\rangle \equiv \frac{1}{\sqrt{2}}(1\ -i\ 0\ 0)^T$; $|R_2\rangle \equiv \frac{1}{\sqrt{2}}(0\ 0\ 1\ i)^T$; $|L_2\rangle \equiv \frac{1}{\sqrt{2}}(0\ 0\ 1\ -i)^T$, the phonon eigenvector ϵ can be represented as

$$\epsilon = \sum_{\alpha=1}^{n} \epsilon_{R_\alpha} |R_\alpha\rangle + \epsilon_{L_\alpha} |L_\alpha\rangle, \tag{1}$$

where $\epsilon_{R_\alpha} = \langle R_\alpha | \epsilon \rangle = \frac{1}{\sqrt{2}}(x_\alpha - iy_\alpha)$, $\epsilon_{L_\alpha} = \langle L_\alpha | \epsilon \rangle = \frac{1}{\sqrt{2}}(x_\alpha + iy_\alpha)$. Then the operator for phonon circular polarization along z direction can be defined as

$$\hat{S}^z \equiv \sum_{\alpha=1}^{n} (|R_\alpha\rangle \langle R_\alpha| - |L_\alpha\rangle \langle L_\alpha|), \tag{2}$$

and the phonon circular polarization equals to

$$s^z_{\rm ph} = \epsilon^\dagger \hat{S}^z \epsilon \hbar = \sum_{\alpha=1}^{n} \left(|\epsilon_{R\alpha}|^2 - |\epsilon_{L\alpha}|^2 \right) \hbar, \tag{3}$$

here $n = 2$ for two-sublattice unit cells. The phonon circular polarization can have a value between $\pm\hbar$ since $\sum_\alpha |\epsilon_{R_\alpha}|^2 + |\epsilon_{L_\alpha}|^2 = 1$. The $s^z_{\rm ph}$ has the same form with that of phonon angular momentum $j^z_{\boldsymbol{k},\sigma}$ along z direction [16] (see Supplementary information Sec. I [15]). The contribution from each sublattice in one unit cell to the phonon circular polarization is s^z_α, which equals to $\epsilon^\dagger \hat{S}^z_\alpha \epsilon \hbar$ with $\hat{S}^z_\alpha = |R_\alpha\rangle \langle R_\alpha| - |L_\alpha\rangle \langle L_\alpha|$. In Fig. 1(a), at valley $\boldsymbol{K}$, $s^z_A = 0$, $s^z_B = -\hbar$ for band 2 while $s^z_A = \hbar$, $s^z_B = 0$ for band 3, where the phonon circular polarization happens to be quantized; for band 1 and 4, sublattice A and B do opposite circular vibration with different magnitude of $s_{A,B}$. Therefore phonon circular polarization $s^z_{\rm ph}$ at valleys can be nonzero. By introducing a staggered sublattice onsite potential, the similar chiral phonons at valleys can also be observed; and the chiral valley phonons can be observed in graphene systems with introducing isotope doping (please see Supplementary information Sec. II and III [15]).

At the zone center $\boldsymbol{\Gamma}$, as shown in Fig. 1(a), there are doubly degenerate acoustic modes (LA and TA) and doubly degenerate optical modes (LO and TO) which are not circularly polarized; however, we can obtain circular polarized phonon modes by superposition of the degenerated modes.

Phonon pseudo angular momentum. In a honeycomb lattice, at high-symmetry points $\boldsymbol{\Gamma}, \boldsymbol{K}, \boldsymbol{K'}$ phonons are invariant under a three-fold discrete rotation about the direction (z) perpendicular to the lattice plane. Under the rotation, one can obtain $\Re(\frac{2\pi}{3}, z)u_{\boldsymbol{k}} = e^{-i\frac{2\pi}{3}l^{\boldsymbol{k}}_{\rm ph}} u_{\boldsymbol{k}}$, where $l^{\boldsymbol{k}}_{\rm ph}$ is defined as the PAM of phonon with wave function $u_{\boldsymbol{k}}$ and has values of ±1 or 0. The phase correlation of the phonon wave function comes from two parts, one is from local (intra-cell) part $\epsilon_{\boldsymbol{k},\sigma}$, another is from the non-local (inter-cell) part $e^{i\boldsymbol{R}_l \cdot \boldsymbol{k}}$. Thus under a three-fold rotation, one can obtain spin PAM l^s for the local part and orbital PAM l^o for the non-local part.

The orbital PAM can be obtained from phase change under a three-fold rotation, which is shown in Fig. 1 (b). We can obtain $l^o_A = \tau$ and $l^o_B = -\tau$, $\tau = \pm1$ labels the two valleys $\boldsymbol{K}$ and $\boldsymbol{K'}$. At $\boldsymbol{\Gamma}$ point, there is no phase change for both sublattices under a three-fold rotation, thus $l^o_A = l^o_B = 0$. Both circular polarization $|R_\alpha\rangle$ and $|L_\alpha\rangle$ are eigenstates of the operator $\Re(\frac{2\pi}{3}, z)$ with PAM $l^s_R = 1$ and $l^s_L = -1$ respectively. Therefore, in Fig. 1(a), at valley $\boldsymbol{K}$, $l^s_A = -1$, $l^s_B = 1$ for band 1 and 4, $l^s_B = -1$ for band 2 and $l^s_A = 1$ for band 3. Since phonon wave function must be an eigenstate of the rotation operator, PAM of phonon equals $l_{\rm ph} = l^s_A + l^o_A = l^s_B + l^o_B$ if both sublattices are vibrating; if one is still, it is decided

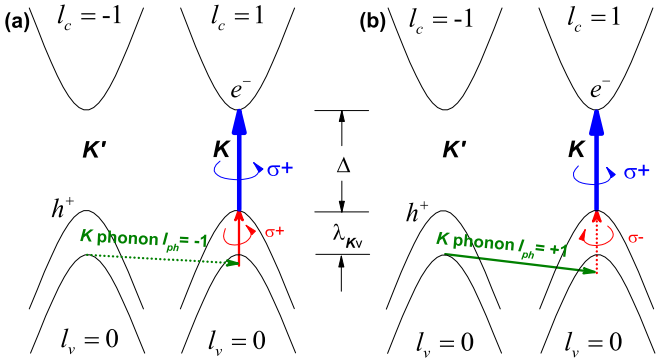

FIG. 2: **Valley phonons emitted in hole intervalley scattering in MoS_2.** The exciton is excited by a right polarized photon with energy (Δ) at $\boldsymbol{K}$ valley. (a) By absorbing a stimulated right-handed photon with energy ($\lambda_{\boldsymbol{K}v} + \hbar\omega$), the excited hole in valence band is scattered to the other valley $\boldsymbol{K}'$ by emitting a valley phonon with energy $\hbar\omega$ and PAM $l_{\rm ph} = -1$. (b) A stimulated left-handed photon is absorbed and a phonon with $l_{\rm ph} = 1$ is emitted. The pseudo angular momenta of electrons in conduction band and valence band ($l_{v(c)} = \pm 1, 0$) are also marked.

by the other vibrating sublattice. Therefore we can obtain phonon PAM as listed in Fig. 1 (c). At $\boldsymbol{\Gamma}$ point, $l_{\rm ph} = l^s_A = l^s_B$ since orbital PAM is zero. By superposition of the doubly degenerated modes, sublattices do the same circular vibration, which can be right-handed or left-handed. Thus the phonon PAM can be ± 1 for doubly degenerated modes.

At high-symmetry points where the three-fold rotational symmetry holds, the PAM of non-degenerate phonon modes must be ± 1 or zero. Since a three-fold rotation center can be chose at any sublattice in a unit cell when the orbital PAM of this sublattice will be zero, the spin PAM of the sublattice must be equal to phonon PAM, that is, it must also be ± 1 or zero. Therefore as shown in Fig. 1(a), for all phonon modes at valleys sublattices must do circularly polarized vibrations otherwise they are still. For three-dimensional vibrations, the out-of-plane modes (ZA or ZO modes) are also an eigenstate of the three-fold rotation with PAM of $l_{\rm ph} = 0$.

Selection rules. For electrons with zero moment along the normal direction of the plane (z), the state is invariant under a three-fold rotation, the PAM is decided by the orbits on sublattice A or B. Based on the lattice structure in Fig. 1 (b), if we assume the valence band corresponds to the orbit on sublattice A and the conduction band corresponds to the orbit on sublattice B, we can obtain all the pseudo angular momenta $l_{c(v)} = \mp\tau$. Therefore, due to conservation of PAM, one can expect an azimuthal selection rule $l_c - l_v = l_{\rm photon} = \pm\tau$ for interband transition by photons with right ($\sigma+$) or left ($\sigma-$) circular polarization in the gapped graphene. The excited electron in the conduction band can have an intravalley scattering by a phonon at Γ, and then combines with the hole in the valence band by emitting another photon. This process is called as the first order Raman scattering (e.g. G-peak in Graphene). In this process, due to the conservation of PAM, we have a selection rule as $\Delta l_{\rm photon} = l_{\rm ph}$. Since the doubly degenerate optical modes at $\boldsymbol{\Gamma}$ are Raman active and have pseudo angular momenta of ± 1, thus we can expect a helicity-resolved Raman G-peak in honeycomb lattices, which can be gapped graphene or boron nitride monolayer. In the whole process, the incident right (left) handed photon absorbs a right (left) handed phonon or emits a left (right) handed phonon then changes its helicity to be a left (right) handed photon. Such selection rule explains the helicity resolved Raman scattering in layered TMD as reported in Ref. [11]. For the out-of-plane phonon involving only chalcogen atoms as well as the low energy breathing modes, they have $l_{\rm ph} = 0$ thus the helicity of the incident photon will not change.

It is well known that in graphene the double resonance D-peak in Raman spectrum is related to phonon modes in the vicinity of the $\boldsymbol{K}$ point during the intervalley scattering [17, 18]. In the intervalley scattering by phonon the whole system has three-fold rotational symmetry, thus we can expect a selection rule from the conservation of PAM, that is $l_{c(v)}(\boldsymbol{K}) - l_{c(v)}(\boldsymbol{K}') = \pm 1$ by emitting a circularly polarized valley phonon ($l_{\rm ph} = \pm 1$), where momentum and energy conservations are also applied. Thus we can expect an valley phonon with a specific PAM can be created. Due to the PAM of valley phonons are different, we can observe a circularly polarized infrared spectrum during the valley phonon interband scattering (please see Supplementary information Sec. IV for the detailed discussion [15]).

With spin-orbit coupling MoS_2 has a bandgap of $\Delta = 1.65$eV and a spin-splitting for the highest valence band at $\boldsymbol{K}$ valley $\lambda_{\boldsymbol{K}v} = 150$ meV as shown in Fig. 2, while for the lowest conductance band there is a 3 meV splitting which can be negligible [21]. With a photon absorbtion or emission we can expect to observe intervalley electron scattering at valley centers involving a valley center phonon, where the selection rules imply $\Delta l_{\rm el} = \pm l_{\rm ph} \pm l_{\rm photon}$ and $\lambda_{\boldsymbol{K}} = \pm\hbar\omega_{\rm ph} \pm \hbar\omega_{\rm photon}$, where '+' means emission and '−' means absorbtion. For monolayer MoS_2, at valleys the PAM of electrons in the conduction band are ± 1 while they are zero for the valence band [4]. Through a right-handed polarized photon a pair of exciton are excited at $\boldsymbol{K}$ valley as shown in Fig. 2, where the blue lines correspond to the absorption of a right-handed photon with energy Δ. Since the excited electron is in the valley center, which cannot be scattered to another valley through emitting a phonon. However, due to the large spin-splitting of valence band the hole can be scattered to another valley by absorbing a stimulated circularly polarized photon and emitting a chiral valley phonon, where the spin of electron is fixed. Us-

TABLE I: **Chiral phonons in K Valley of MoS_2.** Monolayer MoS_2 has 9 modes (n) of phonon with energy $\hbar\omega_{\rm ph}$ (meV), Mo and S are located in A and B respectively as show in Fig. 1 (b) in the main text, thus the orbital PAM $l^o_{\rm Mo}=1$ and $l^o_{\rm S}=-1$. $s^z_{\rm Mo}$ ($s^z_{\rm S}$), $l^s_{\rm Mo}$ ($l^s_{\rm S}$), and $l_{\rm ph}$ are circular polarizations of Mo (S), spin pseudo angular momenta of Mo (S), and phonon PAM. The Mirror symmetry (M_S) is relative to the plane of the monolayer of MoS_2; it is 1 (-1) if the mode is even (odd) under the mirror symmetry operation.

n	$\hbar\omega_{\rm ph}$	$s^z_{\rm Mo}$	$s^z_{\rm S}$	$l^s_{\rm Mo}$	$l^s_{\rm S}$	$l_{\rm ph}$	M_S
1	14.4	0.64	0	1	0	-1	1
2	21.5	0	-0.34	0	-1	1	-1
3	31.9	-0.18	0.41	-1	1	0	1
4	40.0	0	-0.50	0	-1	1	1
5	40.2	0	0	-	-	0	-1
6	41.5	0	0.50	0	1	0	1
7	45.1	0	-0.40	0	-1	1	-1
8	48.0	0.06	0	1	0	-1	1
9	49.2	-0.34	0.33	-1	1	0	1

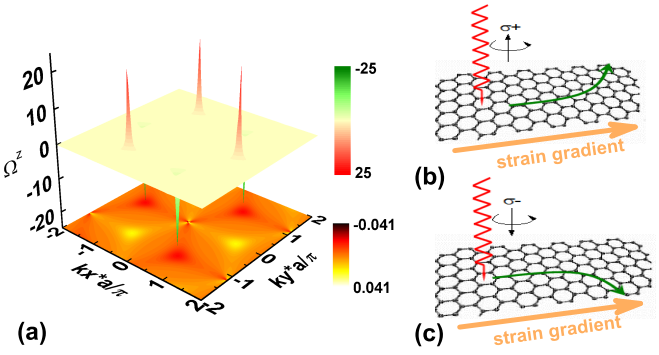

FIG. 3: **Phonon Berry curvature and valley phonon Hall effect in a honeycomb lattice.** (a) Berry curvature of band 1 (bottom contour plot) and band 2 (top 3D plot). Band 3 (Band 4) has phonon angular momentum opposite to that of band 2 (band 1). (b) ((c)) Schematic of valley phonon Hall effect (Hall current denoted by olive curve arrows) under a strain gradient (orange arrows), where valley phonons are excited by a ray of right-handed or left-handed polarized light (red wave lines). The parameters are the same with those in Fig. 1.

ing the Quantum-Espresso code [22], we obtain phonons for all bands at valleys as shown in Table I (please see Supplementary information Sec. V [15]). At $\boldsymbol{K}$ valley, phonons with energy 14.4 and 48.0 meV have PAM of $l_{\rm ph}=-1$ and phonons of 21.5, 40.0 and 45.1 meV have $l_{\rm ph}$ of 1.

As shown in Fig. 2(a), through a stimulated right-handed light scanning on the sample, we can observe certain resonance peak on $\lambda_{\boldsymbol{K}v}+\hbar\omega_{\rm ph}$ where the emitted chiral phonon carries a PAM of $l_{\rm ph}=-1$ at $\boldsymbol{K}$ point due to the selection rules at valleys. The resonance peak is at 164.4 meV (another peak of 198.0 meV is not obvious due to the small polarization of 48.0 meV phonon). And for a stimulated left-handed photon in Fig. 2(b), we can only observe one peak of 190.0 meV correspond to phonon mode of 40.0 meV while the other two modes will not be involved since they are odd under mirror operation (see Table I) since in the scattering process the whole system keeps even under a mirror operation relative to the x-y plane. After scattered by phonon and photon, the pair of electron and hole locate in different valleys which is consistent with the recent founding of low-energy excitons with a large momentum [23]. Similarly, a chiral phonon at $\boldsymbol{K}'$ can be emitted in the scattering of hole of an exciton at $\boldsymbol{K}'$ valley which can be excited by a left-handed photon with 1.65 eV. Therefore, a specific chiral phonon at a definite valley can be obtained through a stimulated photon. With the two-step polarized light shinning on the sample, a large number of valley phonons with definite frequencies can be created.

Valley phonon Hall effect. In the presence of an in-plane electric field, an electron will acquire an anomalous velocity proportional to the Berry curvature in the transverse direction [24, 25]. Recently the electronic valley Hall effect proposed in [1] has been experimentally observed in monolayer MoS_2 transistors [26] and in graphene superlattices [27]. As discussed above, phonons with definite frequencies at a specific valley can be massively created, thus for valley phonons, if its Berry curvature is nonzero we can also expect to observe valley phonon Hall effect in the presence of an in-plane gradient strain field. Such valley phonon Hall effect can provide us another way to observe valley phonons.

With the breaking of spatial inversion symmetry we observe nonzero phonon Berry curvature at valleys as shown in Fig. 3 (a) (see Supplementary information Sec. VI for derivation [15]). Band 2 and band 3 have large Berry curvatures at valleys, while those of band 1 and 4 are small. Due to the nonzero phonon Berry curvature, applying a strain gradient $\boldsymbol{E}_{\rm strain}$ along x direction, phonons excited at a different valley will go to a different transverse direction since $\boldsymbol{v}_{\rm anom}\propto-\boldsymbol{E}_{\rm strain}\times\boldsymbol{\Omega}$ in analogy to electrons. If the photon polarization is reversed, the transverse phonon current would be reversed as shown in Fig. 3 (b) and (c). With the accumulation of phonons on one edge, people can measure a temperature difference along the transverse direction. The temperature difference changes sign if the circular polarization of the stimulated photon is reserved. Phonon Hall effect has been observed in a paramagnetic insulator [28] where a magnetic field can distort phonon transport thus a transverse temperature difference can be observed, which has attracted many studies in this field [29–31]. The Berry curvature induced transverse valley phonon Hall effect at nonmagnetic systems with inversion symmetry broken would attract new applications.

We thank Ji Feng and Gang Zhang for helpful discussions. We acknowledge support from DOE-DMSE (DE-FG03-02ER45958),NBRPC (2012CB-921300), NSFC (91121004,11574154), and the Welch Foundation (F-1255).

[1] D. Xiao, W. Yao, and Q. Niu, Phys. Rev. Lett. **99**, 236809 (2007).
[2] W. Yao, D. Xiao, Q. Niu, Phys. Rev. B **77**, 235406 (2008).
[3] D. Xiao, G.-B. Liu, W. Feng, X. Xu, and W. Yao, Phys. Rev. Lett. **108**, 196802 (2012).
[4] T. Cao, *et al.*, Nat. Comms **3**, 887 (2012).
[5] Q. H. Wang, K. Kalantar-Zadeh, A. Kis, J. N. Coleman, and M. S. Strano, Nat. Nano. **7**, 699 (2012).
[6] K. F. Mak, K. He, J. Shan, and T. F. Heinz, Nat. Nano. **7**, 494 (2012).
[7] H. Zeng, J. Dai, W. Yao, D. Xiao and X. Cui, Nat. Nano. **7**, 490 (2012).
[8] S. Wu, *et al.*, Nat. Phys. **9**, 149 (2013).
[9] A. M. Jones, *et al.*, Nat. Nano. **8**, 634 (2013).
[10] X. Xu, W. Yao, D. Xiao, and T. F. Heinz, Nat. Phys. **10**, 343 (2014).
[11] S.-Y. Chen, C. Zheng, M. S. Fuhrer, and J. Yan, Nano Lett., 15, 2526 (2015).
[12] S. Chen, *et al.*, Nat. Mater. **11** 203 (2012).
[13] S. Y. Zhou, *et al.*, Nat. Mater. **6**, 770 (2007).
[14] G. Kim, *et al.*, Nano Lett., **13** , 1834 (2013).
[15] See Supplemental Material at http://link.aps.org/supplemental/10.1103/PhysRevLett.115.... for details, which includes Refs. [32–34].
[16] L. Zhang and Q. Niu, Phys. Rev. Lett. **112**, 085503 (2014).
[17] R. Saito, *et al*, Phys. Rev. Lett. **88**. 027401 (2001).
[18] L. M. Malarda, M. A. Pimentaa, G. Dresselhaus, M. S. Dresselhaus, Phys. Rep. **473**, 51 (2009).
[19] W. Liu, W. Cao, J. Kang, and K. Banerje, ECS Transactions, **58**, 281 (2013).
[20] H. Terrones, *et al.*, Sci. Rep. **4**, 4215 (2013).
[21] Z. M. Wang, *MoS_2: Materials, Physics, and Devices* (Springer. Switzerland. 2014).
[22] P. Giannozzi, *et al.*, J. Phys.: Condens. Matter **21**, 395502 (2009).
[23] F. Wu, F. Qu, and A. H. MacDonald, Phys. Rev. B 91, 075310 (2015).
[24] M.-C. Chang and Q. Niu, Phys. Rev. B **53**, 7010 (1996).
[25] D. Xiao, M.-C. Chang and Q. Niu, Rev. Mod. Phys. **82**, 1959 (2010).
[26] K. F. Mak, K. L. McGill, J. Park, P. L. McEuen, Science **344**, 1489 (2014).
[27] R. V. Gorbachev, *et al.*, Science 346, **448** (2014).
[28] C. Strohm, G. L. J. A. Rikken, and P. Wyder Phys. Rev. Lett. **95**, 155901 (2005); A. V. Inyushkin and A. N. Taldenkov, JETP Lett. **86**, 379 (2007).
[29] L. Sheng, D. N. Sheng, and C. S. Ting, Phys. Rev. Lett. **96**, 155901 (2006); Y. Kagan and L.A.Maksimov, Phys. Rev. Lett. **100**, 145902 (2008);
[30] J.-S. Wang and L. Zhang, Phys. Rev. B **80**, 012301 (2009); L. Zhang, J.-S. Wang, and B. Li, New J. Phys. **11**, 113038 (2009); L. Zhang, J. Ren, J.-S. Wang, and B. Li, Phys. Rev. Lett. **105**, 225901 (2010); B. K. Agarwalla, L. Zhang, J.-S. Wang, B. Li, Eur. Phys. J. B **81**, 197 (2011); L. Zhang, J. Ren, J.-S. Wang, and B. Li, J. Phys.: Cond. Matt. **23**, 305402 (2011);
[31] T. Qin, J. Zhou, and J. Shi, Phys. Rev. B 86, 104305 (2012); M. Mori, A. S.-Smith, O. P. Sushkov, and S. Maekawa, Phys. Rev. Lett. 113, 265901(2014).
[32] R. Saito,, Dresselhaus, G.and Dresselhaus, M. S. Physical Properties of Carbon Nanotubes. (Imperial College Press, London, 1998).
[33] J. Callaway, Quantum Theory of the Solid State, 2nd ed. (Academic Press, San Diego, 1991).
[34] G. Giovannetti, Phys. Rev. B **76**, 073103 (2007).